Neurobiology of Disease 89 (2016) 157–168

Contents lists available at ScienceDirect

Neurobiology of Disease

journal homepage: www.elsevier.com/locate/ynbdi

Astrocyte membrane properties are altered in a rat model of developmental cortical malformation but single-cell astrocytic glutamate uptake is robust

Elizabeth Hanson [a,b], Niels Christian Danbolt [c], Chris G. Dulla [a,b,*]

[a] Department of Neuroscience, Tufts University School of Medicine, 136 Harrison Avenue, Boston, MA 02111, USA
[b] Neuroscience Program, Tufts Sackler School of Biomedical Sciences, 136 Harrison Avenue, Boston, MA 02111, USA
[c] Department of Molecular Medicine, Institute of Basic Medical Sciences, University of Oslo, P.O. Box 1105 Blindern, N-0317 Oslo, Norway

ARTICLE INFO

Article history:
Received 22 September 2015
Revised 3 February 2016
Accepted 9 February 2016
Available online 10 February 2016

Keywords:
Epilepsy
Cortical malformation
Glutamate
Glutamate transport
GLT-1
GLAST
EAAT1
EAAT2
Membrane resistance
Glial development

ABSTRACT

Developmental cortical malformations (DCMs) are linked with severe epilepsy and are caused by both genetic and environmental insults. DCMs include several neurological diseases, such as focal cortical dysplasia, polymicrogyria, schizencephaly, and others. Human studies have implicated astrocyte reactivity and dysfunction in the pathophysiology of DCMs, but their specific role is unknown. As astrocytes powerfully regulate glutamate neurotransmission, and glutamate levels are known to be increased in human epileptic foci, understanding the role of astrocytes in the pathological sequelae of DCMs is extremely important. Additionally, recent studies examining astrocyte glutamate uptake in DCMs have reported conflicting results, adding confusion to the field. In this study we utilized the freeze lesion (FL) model of DCM, which is known to induce reactive astrocytosis and cause significant changes in astrocyte morphology, proliferation, and distribution. Using whole-cell patch clamp recording from astrocytes, we recorded both UV-uncaging and synaptically evoked glutamate transporter currents (TCs), widely accepted assays of functional glutamate transport by astrocytes. With this approach, we set out to test the hypothesis that astrocyte membrane properties and glutamate transport were disrupted in this model of DCM. Though we found that the developmental maturation of astrocyte membrane resistance was disrupted by FL, glutamate uptake by individual astrocytes was robust throughout FL development. Interestingly, using an immunolabeling approach, we observed spatial and developmental differences in excitatory amino acid transporter (EAAT) expression in FL cortex. Spatially specific differences in EAAT2 (GLT-1) and EAAT1 (GLAST) expression suggest that the relative contribution of each EAAT to astrocytic glutamate uptake may be altered in FL cortex. Lastly, we carefully analyzed the amplitudes and onset times of both synaptically- and UV uncaging-evoked TCs. We found that in the FL cortex, synaptically-evoked, but not UV uncaging-evoked TCs, were larger in amplitude. Additionally, we found that the amount of electrical stimulation required to evoke a synaptic TC was significantly reduced in the FL cortex. Both of these findings are consistent with increased excitatory input to the FL cortex, but not with changes in how individual astrocytes remove glutamate. Taken together, our results demonstrate that the maturation of astrocyte membrane resistance, local distribution of glutamate transporters, and glutamatergic input to the cortex are altered in the FL model, but that single-cell astrocytic glutamate uptake is robust.

1. Introduction

Developmental cortical malformations (DCMs) are a common cause of intractable epilepsy and are linked to environmental and genetic insults occurring in utero or during early post-natal development (Guerrini and Dobyns, 2014; Jacobs et al., 1999b; Palmini et al., 1995). DCMs include focal cortical dysplasia, polymicrogyria, and schizencephaly, all of which are characterized by disorganized cortical architecture and severe, often intractable, epilepsy (Barkovich et al., 2005; Raymond et al., 1995; Sisodiya, 2000; Tassi et al., 2002). The molecular, cellular, and network level changes that make the malformed brain prone to ictogenesis are largely unknown. Changes in neuronal morphology and location, synapse number and function, and neurotransmitter receptor expression and localization have all been reported in different DCMs and may be mechanistically linked to cortical hyperexcitability (reviewed by Marin-Valencia et al. (2014) and Aronica et al. (2012)). Changes in astrocyte properties are also of great interest in understanding the pathogenesis of DCMs.

Astrocytes remove the bulk of extracellular glutamate (Holmseth et al., 2012a; Petr et al., 2015) and buffer extracellular potassium in

* Corresponding author at: Tufts Sackler School of Biomedical Sciences, South Cove 203, 136 Harrison Avenue, Boston, MA 02111, USA.
Available online on ScienceDirect (www.sciencedirect.com).

http://dx.doi.org/10.1016/j.nbd.2016.02.012
0969-9961/

tiled, non-overlapping domains (Halassa et al., 2007). Glutamate uptake by astrocytes is mediated by the excitatory amino acid transporters (EAATs), GLT-1 and GLAST. EAATs are sodium-dependent and can rapidly bind and transport glutamate into astrocytes (Danbolt, 2001). EAATs are developmentally regulated, greatly increasing their expression during development (Ullensvang et al., 1997). The proper function of EAATs ensures rapid clearing of extracellular glutamate, limits post-synaptic glutamate receptor activation, and enables recycling of glutamate (Fonnum, 1984; Oliet et al., 2001; Petroff et al., 2002). In the injured or epileptic brain, astrocytes become reactive and many of their properties are disrupted. Reactive astrocytes express high levels of glial fibrillary acidic protein (GFAP), have hypertrophied morphology, and exhibit an altered protein expression profile (reviewed by Sofroniew (2009)). Functional glutamate transport may also be disrupted, though changes in glutamate transporter expression in reactive astrocytes remain debatable. In human DCMs, astrocytes are often reactive (Kakita et al., 2004) and GLT-1 expression has been reported to be decreased (Ulu et al., 2010). Importantly, elevated extracellular glutamate levels have been reported in human epileptic foci (Cavus et al., 2005), suggesting that glutamate is dysregulated and that lowering glutamate levels may be a therapeutic target for DCM-associated hyperexcitability.

To better understand the role of glutamate uptake in the pathogenesis of DCMs, we have utilized the freeze lesion (FL) model of DCM. In the FL model, a freezing probe is placed on the skull of a rat pup on the day of birth (P0) resulting in the formation of a cortical microgyrus (Dvorák and Feit, 1977). The microgyrus is bordered both medially and laterally by normally-laminated cortex. This normally-laminated cortex surrounding the microgyrus forms the paramicrogyral zone (PMZ). The PMZ is known to be hyperexcitable beginning approximately two weeks following FL (Jacobs et al., 1996). Electrical stimulation of ascending cortical axons generates epileptiform, polyphasic cortical field potentials in the PMZ (Hablitz and DeFazio, 1998). Interestingly, cortical field potentials recorded in the microgyrus are not epileptiform, indicating heterogeneity in the malformed and surrounding tissue (Dulla et al., 2012; Jacobs et al., 1999a). In vivo, FL animals have an enhanced response to kainic acid treatment (Andresen et al., 2014) and, when given multiple FL, animals have spontaneous seizures (Kamada et al., 2013). Although the FL does not etiologically replicate human DCMs, it does provide an excellent opportunity to probe the molecular and cellular consequences of neonatal injury prior to the onset of network dysfunction in a model of DCM.

Because DCMs arise in the developing brain (both in humans and in animal models), astrocytes are exposed to injury before they are fully matured (Morel et al., 2014). Thus, astrocyte development is disrupted by FL, likely resulting in altered functional maturation of glutamate uptake. However, characterizing the function of individual astrocytes in DCM is complicated by astrocyte reactivity, proliferation, and heterogeneity following injury (Bordey et al., 2001; Shimizu-Okabe et al., 2007). Perhaps because of this, studies of astrocytic glutamate uptake in FL cortex have reached conflicting conclusions. Specifically, studies have shown that the effects of the EAAT inhibitor DL-*threo*-β-benzyloxyaspartate (TBOA) on network activity are potentiated following FL. Additionally, blockade of EAATs evokes spontaneous network discharges in FL but not in sham-injured cortex (S. L. Campbell and Hablitz, 2008). Furthermore, a recent study has shown that the amplitude of glutamate transporter currents is decreased in individual PMZ astrocytes (Campbell et al., 2014). These studies concluded that glutamate uptake is decreased, thus increasing glutamate accumulation in the extracellular space and contributing acutely to hyperexcitability. However, recent work from our group has demonstrated intact astrocytic glutamate uptake in the PMZ and suggested that FL specifically affects the developmental switch from GLAST-mediated to GLT-1-mediated uptake (Armbruster et al., 2014). We also showed that the local density of astrocytes is decreased in the PMZ and that the functional domain of astrocytes is increased. This suggests that there may be disruptions in astrocyte territories which may lead to subsequent disruptions in their homeostatic functions (Armbruster et al., 2014; Dulla et al., 2012). Finally, it remains unclear how alterations in astrocyte coverage or function during the FL latent period influence network development. Thus, questions remain about whether an alteration in glutamate uptake contributes to the development of hyperexcitable neuronal networks in a model of developmental cortical malformation, and whether a reduction in glutamate uptake contributes acutely to hyperexcitability.

In this study, we seek to determine whether the maturation and function of individual astrocytes is disrupted by FL, potentially contributing to pathological network development and hyperexcitability in the mature malformed cortex. We use whole-cell astrocyte electrophysiology to measure astrocytic membrane resistance in lesioned cortex before and after the onset of hyperexcitability, simultaneously measure uncaging-evoked glutamate transporter currents in the same astrocytes, compare synaptically-released to uncaging-evoked glutamate transients in the mature FL cortex, and examine glutamate transporter immunoreactivity throughout lesion development. We demonstrate that the rate of glutamate clearance is unchanged by FL both before and after the onset of hyperexcitability, though astrocyte membrane resistance is altered during the latent period, at postnatal day (P) 7. Interestingly, we find that synaptically-activated transporter current (STC) are larger in amplitude and more easily evoked in the FL cortex. Our findings suggest that decreased astrocytic uptake may not contribute significantly to acute PMZ hyperexcitability and they support the idea that hyperexcitability in the mature PMZ is caused by increases in excitatory input.

2. Materials and methods

2.1. Animals and freeze lesion surgery

Experimental microgyri in primary somatosensory cortex (left hemisphere) were induced in P0 Sprague–Dawley rat pups (Jackson Laboratories) by freeze lesioning as described previously (Jacobs and Prince, 2005). All protocols were approved by the Tufts Institutional Animal Care and Use Committee. Briefly, animals were anesthetized by hypothermia, an incision into the scalp was made, and a 5×2 mm copper probe cooled to -50 to -60 °C was placed onto the exposed skull for 5 s (approx. 1 mm right of midline, between bregma and lambda). Sham operated littermates were generated in a similar manner with a room temperature probe. After freeze-lesioning, the incision was closed using surgical glue, and pups were warmed and returned to the dam. At approximately two weeks of age, a fully formed microgyrus was present.

2.2. Slice preparation

Cortical brain slices, 400 μm thickness, containing the sensorimotor cortex were prepared from P6–8 and P27–33 Sprague–Dawley rats of either sex. Rats were anesthetized with isoflurane, decapitated, and the brains were rapidly removed and placed in cold slicing solution (in mM): 2.5 KCl, 1.25 NaH_2PO_4, 10 $MgSO_4$, 0.5 $CaCl_2$, 11 glucose, 234 sucrose, and 26 $NaHCO_3$, equilibrated with 95% O_2:5% CO_2. The brain was glued to a Vibratome VT1200S (Leica) and slices were cut in a coronal orientation. Slices were then placed into a recovery chamber containing artificial cerebrospinal fluid (aCSF, in mM: 126 NaCl, 2.5 KCl, 1.25 NaH_2PO_4, 1 $MgSO_4$, 2 $CaCl_2$, 10 glucose, and 26 $NaHCO_3$ equilibrated with 95% O_2:5% CO_2) and 0.5 mM sulforhodamine 101 (SR-101) for 5 min at 32 °C. Following SR-101 incubation, slices were equilibrated in ACSF at 32 °C for 1 h. Slices were allowed to return to room temperature and used for electrophysiology.

2.3. Whole cell recording from astrocytes

Whole-cell patch clamp recordings were made as described previously (Hanson et al., 2015). Astrocytes were identified 1) in deep cortical layers (layers IV-VI) of the paramicrogyral zone (PMZ), 2) in the microgyral zone, and 3) in isotopic cortical areas of sham-lesioned animals. The microgyral zone was visually identified as the cortical area between the lesion midline and the microgyral border and the PMZ was defined as the normally laminated cortex within 1 mm of the microgyrus border (Fig. 1A). Brain slices were placed into a submersion chamber (Siskiyou, OR), held in place with small gold wires, and perfused with aCSF at physiological temperature (32 °C) at a flow rate of 2 ml/min. Astrocytes were identified by morphology (small, round cell bodies) and SR-101 labeling (Nimmerjahn et al., 2004) as imaged with a Cy3 filter cube (excitation 560/40 nm, emission 630/75 nm, Chroma, VT) on an Olympus BX51 microscope equipped with differential interference contrast optics. Astrocyte internal solution contained (in mM) 120 potassium gluconate, 20 HEPES, 10 EGTA, 2 MgATP, and 0.2 NaGTP. 4–12 MΩ borosilicate pipettes were utilized to establish whole cell patch-clamp recordings using a Multiclamp 700B patch clamp amplifier (Molecular Devices, CA), sampled at 10 kHz using pClamp software. Once a whole-cell recording was established, cells were confirmed as astrocytes based on their passive membrane properties, low membrane resistance, and hyperpolarized resting membrane potential. Membrane and access resistance were established by running a membrane test protocol in voltage-clamp configuration. While holding the astrocyte at −80 mV, a 50 ms, +1 mV membrane step was applied and the resultant current was averaged over 100 sweeps. This data was used to calculate membrane resistance (R_m) and access resistance (R_a). A 5 mV, 50 ms depolarizing pulse was applied 500 ms before uncaging or electrical stimulation in order to normalize evoked transporter currents for changes in R_a commonly associated with recording from astrocytes (Diamond et al., 1998). For analysis involving transporter current amplitude, R_m was corrected for on a cell-by-cell basis (Armbruster et al., 2014). A voltage/current (V/I) curve was also generated for each cell in current clamp configuration using a current injection protocol (−300 to 650 pA for 250 ms in 50 pA increments). V/I curves were generated for each cell within 120 s of breaking in to minimize the effects of internal solution dialysis on the measurement of the resting potential.

2.4. Flash-evoked transporter current (FTC) recording

In astrocytes identified by SR-101 and a linear voltage/current relationship, TCs were recorded similar to previous studies (Diamond, 2005). Slices were perfused with aCSF containing 2 mM 4-Methoxy-7-

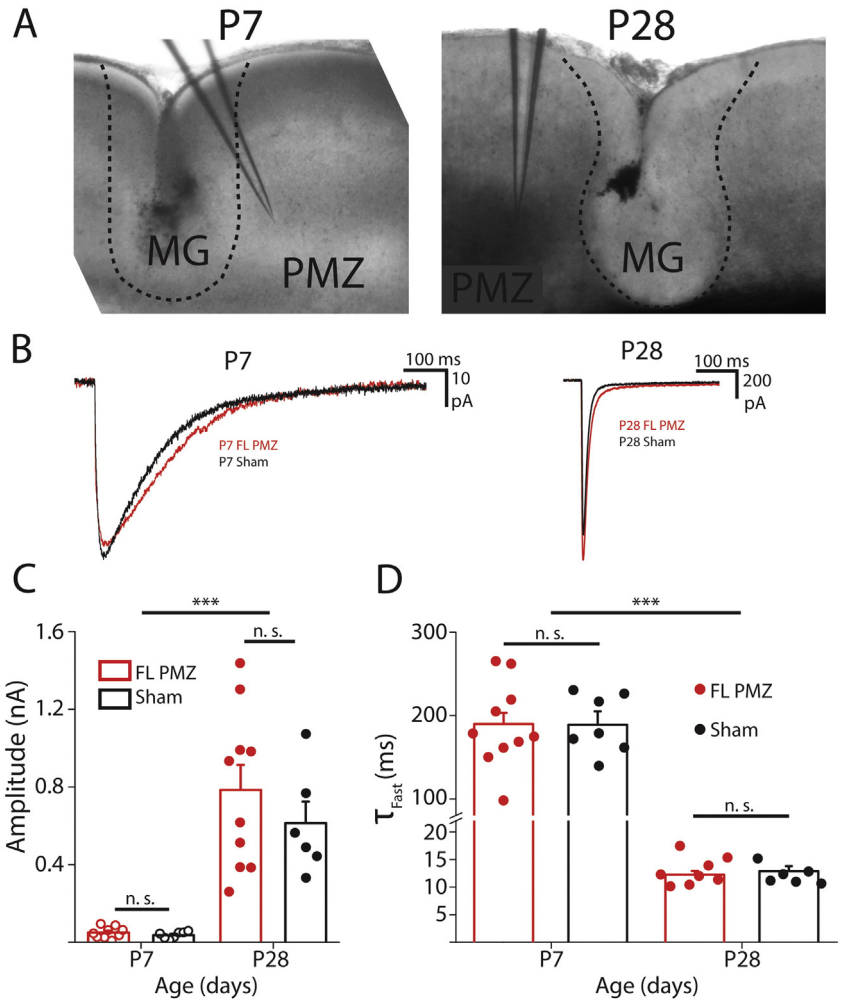

Fig. 1. Glutamate uncaging-evoked transporter currents are not altered by FL. A, 4× magnification DIC images of FL sections used for electrophysiology at P7 and P28. Dashed lines show border of microgyrus. The microgyral zone (MG), paramicrogyral zone (PMZ), and typical electrode placement are shown. B, Representative glutamate transporter currents (TCs) from P7 (left) and P28 (right) sham-injured (black) and P7 FL PMZ astrocytes (red). C, Amplitudes of flash-evoked transporter currents at P7 and P28 from FL PMZ (red) and sham-injured astrocytes (black). D, Average and individual time constants of TC decays at P7 and P8 in FL PMZ (red) and sham-injured cortical astrocytes (black). Error bars represent SEM, ***$p < 0.001$, two-sample t test.

nitroindolinyl-caged-L-glutamate (MNI glutamate, photo-activated glutamate), 10 μM SR-95531(gabazine, antagonist of $GABA_A$ receptors), 20 μM 6,7-dinitroquinoxaline-2,3-dione (DNQX, antagonist of AMPA receptors), and 10 μM 3-(2-Carboxypiperazin-4-yl)propyl-1-phosphonic acid (CPP, antagonist of NMDA receptors), which was oxygenated and circulated at 2 ml/min at 34 °C. FTCs were activated by photostimulation using a 100 mW 355 nm ultra violet (UV) uncaging laser with 10 μm full width at half maximum (FWHM) spot size (Prairie Technologies, Photoactivation System, WI). Laser exposure times were controlled using a fast shutter (Sutter Instruments, CA). In voltage-clamp mode, whole-cell patch clamped astrocytes were maintained at −80 mV. To record FTCs, each sweep contained a + 5 mV, 20 ms voltage step, followed 40 ms later by a 1 ms UV uncaging pulse. Laser light was delivered via an Olympus 60×/N.A. 0.9 water immersion objective (LUMPLANFLN 60XW). After at least 5 sweeps, TBOA (100 μM) was washed on to isolate the transporter current. Currents for individual cells and (representative example in Fig. 6A) are averages of at least 5 consecutive sweeps with the average of 5 sweeps in TBOA subtracted.

2.5. Synaptically-evoked transporter current (STC) recording

In astrocytes identified by SR-101 and a linear voltage/current relationship, STCs were recorded similarly to previous studies (Campbell et al., 2014). Because STC recordings were performed in the presence of Ba^{2+} which precipitates with SO_4, for STC recording aCSF containing $MgPO_4$ in place of $MgSO_4$ was used. Slices were perfused with aCSF containing (in mM) 0.1 $BaCl_2$, 2 mM 4-Methoxy-7-nitroindolinyl-caged-L-glutamate (MNI glutamate, photo-activated glutamate), 10 μM SR-95531 (gabazine, antagonist of GABAA receptors), 20 μM 6,7-dinitroquinoxaline-2,3-dione (DNQX, antagonist of AMPA receptors), and 10 μM 3-(2-Carboxypiperazin-4-yl)propyl-1-phosphonic acid (CPP, antagonist of NMDA receptors), which was oxygenated and circulated at 2 ml/min at 34 °C. STCs were evoked with a bipolar stimulating electrode placed in the white matter below the recoding pipette (Fig. 5A). 50 μs current pulses were used at a stimulation frequency of 0.1 Hz. Stimulation intensity was controlled manually with a stimulus isolation unit (A. M. P. I.). Threshold stimulation intensity was determined for individual astrocytes as the minimum current pulse required to evoke a resolvable TC (5–15 pA, Fig. 5D) and varied from 5 to 500 μA (Fig. 5C). In voltage-clamp mode, whole-cell patch clamped astrocytes were held at −80 mV. To record STCs, each sweep contained a + 5 mV, 20 ms voltage step, followed 250 ms later by a 2× threshold, 50 μs electrical stimulation. After at least 5 sweeps, TBOA (100 μM) was washed on to further isolate the transporter current. Currents for individual cells and representative current shown in Fig. 6A are averages of at least 5 consecutive baseline sweeps with the average of 5 sweeps in TBOA subtracted. Currents shown in Fig. 4B and 5A are TBOA-subtracted averages across cells and the shaded area shows ± SEM.

2.6. Drugs

All salts and glucose for buffers were obtained from Sigma-Aldrich (St. Louis, MO) unless otherwise noted. TBOA, CPP, DNQX, and Gabazine (SR-95531) were obtained from Tocris (St. Louis, MO), maintained as 1000× stock in dimethyl sulfoxide (DNQX, TBOA) or in water (CPP, Gabazine). Dimethyl sulfoxide final concentration was 0.1% in DNQX and increased to 0.2% upon application of TBOA.

2.7. Immunofluorescence

FL and sham-injured rats at ages P7, P14, and P28 were anesthetized, perfused with saline followed by 4% freshly depolymerized paraformaldehyde, decapitated, and brains were dissected and placed in 4% formaldehyde for 12–18 h. Fixed brains were then cryo-protected in a high sucrose solution (in mM: 818 sucrose, 77 sodium phosphate, 23 sodium phosphate), and later sectioned into 40 μm slices using a Thermo Fisher Microm HM 525 cryostat. Brain sections were placed in blocking buffer (5% normal goat serum, 1% bovine serum albumin, in phosphate buffered saline (PBS)) for 1 h at room temperature. GFAP (1:1000, Abcam) and either GLT-1 (0.2 μg/ml Ab#360, (Holmseth et al., 2012b)) or GLAST (1.2 μg/ml Batch Ab#314 (Holmseth et al., 2009)) antibodies were diluted in PBS with 2% Triton-X 100 and 5% blocking buffer. Brain sections were incubated with diluted primary antibodies for 12 h at 4 °C. Brain sections were then rinsed three times in PBS, and secondary antibodies (goat anti-rabbit Alexa 488, Jackson Labs, and goat anti-mouse Cy3.5, Jackson Labs; diluted 1:500 in PBS with 5% blocking buffer) were added to the sections for 2 h at room temperature. FL and sham cortex samples were stained in parallel and carried out in three batches. Slices were mounted using Vectashield (Vector Labs) and imaged with a 20× objective on a Keyence epifluorescence microscope. Raw images were analyzed with ImageJ. 500–800 μm line scans were taken laterally through layers IV-VI to quantify GLT-1 and GLAST expression. In FL cortex, line scans started at the midline of the microgyrus; in sham-injured cortex, line scans started in isotopic cortex. In FL and shams, line scans traveled from the starting point away from the midline of the cortex. GLT-1 and GLAST expression in FL and sham-injured cortex were normalized to the batch average fluorescence of sham-injured cortex, allowing for comparisons of relative fluorescence between FL and shams at each age.

2.8. Statistical analysis

Statistical significance for all experiments was determined using Student's unpaired and paired t-tests as well as ANOVA, as appropriate. All data is presented as the mean ± SEM.

3. Results

3.1. Astrocyte glutamate transporter currents are unaltered by freeze lesion both before and after the onset of hyperexcitability

To directly test whether freeze lesion (FL) alters the functional uptake of glutamate by astrocytes, we recorded glutamate transporter currents (TCs) from astrocytes in FL and sham-injured cortex both at P7 (before the onset of epileptiform activity) and at P28 (after the onset of epileptiform activity). Astrocytes were identified by SR-101 loading (note: using SR-101 to identify astrocytes may lead to selection of only certain sub-types of cells, please see discussion). Whole-cell patch clamp recordings were established in astrocytes in layer V of the paramicrogyral zone (PMZ) in FL animals and in isotopic cortex from sham-injured control rats. TCs were evoked by localized UV-photolysis of MNI-glutamate (glutamate uncaging, 1 ms UV pulse). TC decay kinetics reflect the rate of glutamate clearance from the extracellular space; when glutamate clearance is rapid, TCs have very rapid decay times. As previously reported, glutamate uncaging-evoked TCs are largely uncontaminated by potassium conductances associated with TCs evoked by electrical stimulation. Using this approach, we found no significant changes in TC kinetics or amplitude between FL and shams at either P7 or P28 (P7: $n = 7–9$, $p = 0.68$; P28: $n = 6–10$, $p = 0.38$; Fig. 1B, C). This suggests that the rate of glutamate clearance is unaffected by FL during the latent period and in the mature FL cortex. Consistent with past work, TC amplitude increased and decay times decreased significantly in both groups between P7 and P28 due to developmental increases in EAAT expression.

3.2. Membrane resistance of immature astrocytes is decreased following FL

We next examined whether astrocytic membrane resistance (R_m) was altered by FL either before or after the onset of hyperexcitability. Astrocytes were patch-clamped in FL and sham-injured littermates at either P6-P8 or P27-P30 as in TC experiments. In current clamp configuration, current steps (−350 to 600 pA, 50 pA increments) were

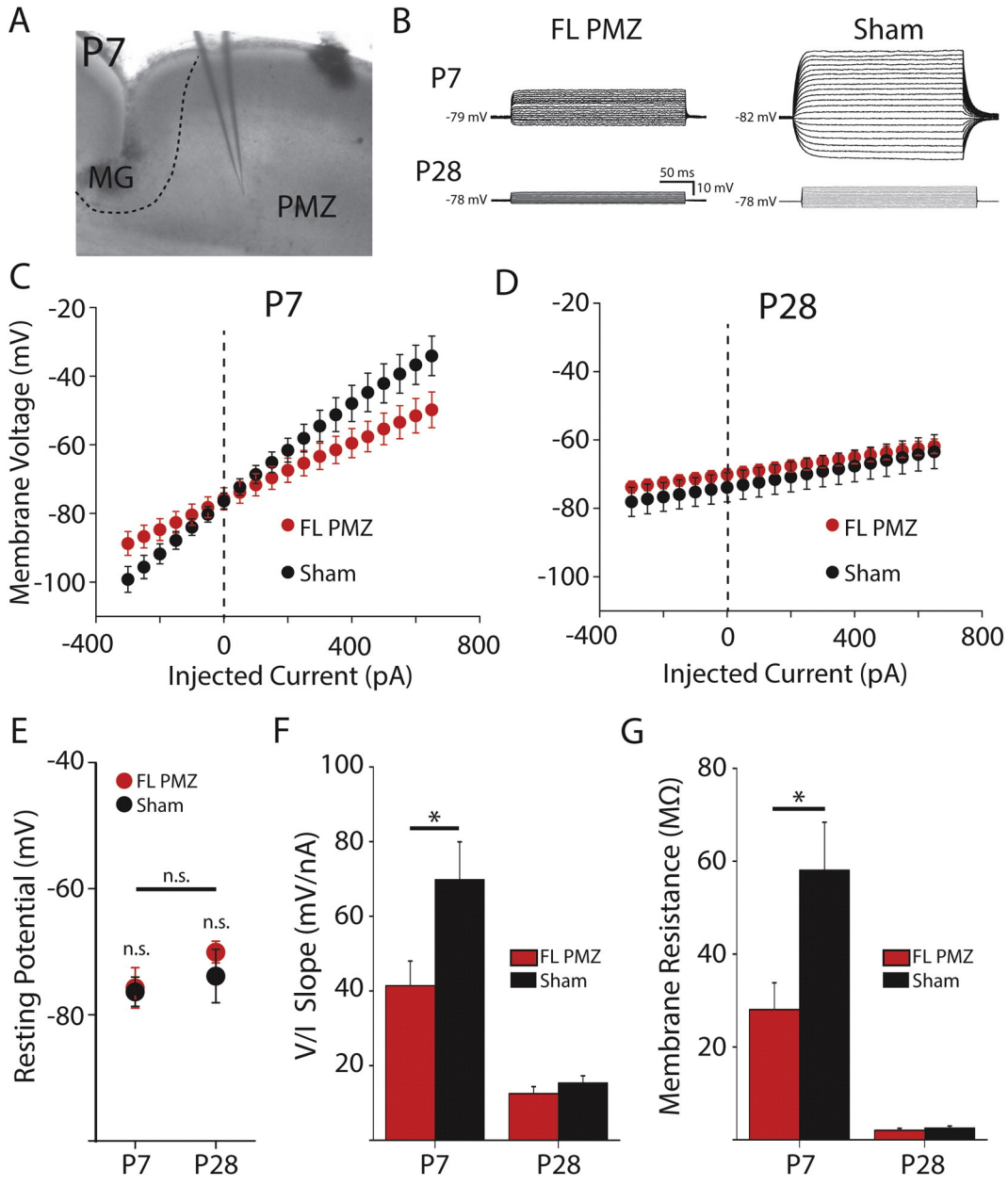

Fig. 2. Astrocyte membrane resistance is decreased in the paramicrogyral zone at P7. A, DIC image of a P7 coronal slice showing the microgyrus (MG), the paramicrogyral zone (PMZ), and the recording electrode in PMZ. B, Overlaid voltage responses in astrocytes current-clamped and injected with 20 current steps from −300 to +160 pA. C, Average voltage/current relationship for astrocytes in freeze lesion (FL) PMZ cortex (red) and sham-injured cortex (black) at P7. D, Same as (C) at P28. E, Resting membrane potentials at P7 and P28 for FL PMZ (red) and sham-injured astrocytes (black). F, Average slopes of the voltage/current relationships in (C) and (D). G, Membrane resistances of astrocytes at P7 and P28 from FL PMZ (red) and sham-injured cortex (black). Error bars represent SEM, *$p < 0.05$, two-sample t-test.

injected and voltage responses were measured (Fig. 2B–D). After switching to voltage-clamp configuration, astrocytes were next held at −80 mV, and subjected to brief positive voltage steps to directly assess membrane and access resistance. All astrocytes recorded at P7 and P28 in PMZ and isotopic sham-injured cortex ($n = 31$) showed linear voltage responses to current injections (Fig. 2C, D) and had similar hyperpolarized resting membrane potentials (P7 PMZ: -75.7 ± 3.22, $n = 9$; P7 sham: -76.4 ± 2.32, $n = 7$; P28 PMZ: -70.1 ± 1.73, $n = 8$; P28 sham: -73.9 ± 4.24; Fig. 2E). At P7, FL significantly decreased the voltage/current (V/I) slope (PMZ: 41 ± 7 mV/nA, sham: 70 ± 10 mV/nA, $p < 0.05$, Fig. 2F) and R_m (PMZ: 28.1 ± 5.78 MΩ, sham: 58.1 ± 10.3 MΩ, $p < 0.05$, Fig. 2C, F, G) in PMZ astrocytes as compared to sham. We previously reported that the R_m of cortical astrocytes decreases substantially over postnatal development. In agreement with this, both the slope of the V/I relationship, reflecting the sum of access and membrane resistance (P28 PMZ: 13 ± 2; P28 Sham: 15 ± 2) and a direct calculation of R_m (P28 PMZ: 2.06 ± 0.38; P28 Sham: 2.57 ± 0.41) for PMZ and sham-injured astrocytes decreased from P7 to P28 (PMZ and sham, $p < 0.05$). Interestingly, by P28, the differences in V/I slope and R_m between PMZ and sham-injured astrocytes were no longer present ($p = 0.30$, Fig. 2D, F, G). Of note, the combination of stable TC decays (Fig. 1) and decreased R_m (Fig. 2) in P7 FL astrocytes suggests the possibility of upregulation in surface levels of glutamate transporters.

Importantly, TC kinetics may be distorted by a number of factors including astrocyte R_m. Therefore, it is important to isolate the glutamate

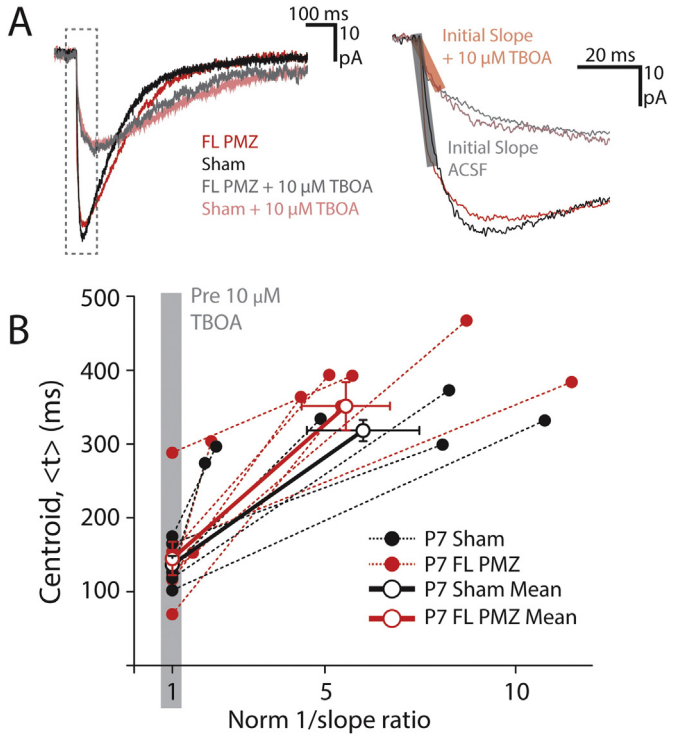

Fig. 3. Membrane resistance filtering does not mask slowing of TCs in P7 FL cortex. A, TCs from a P7 sham-injured (black) and a P7 FL PMZ astrocyte (red) before the wash on of 10 μM (low dose) TBOA (dark) and after low dose TBOA wash on (light). Dashed box (left) outlines the rising phase of the current expanded (right) to show the initial slope of the current (transparent red and black boxes). B, Centroids of TCs before and after the wash on of low dose TBOA (<t>) plotted against the inverse of the initial slopes normalized to the pre-TBOA initial slope (1/slope ratio). Solid circles show individual data points for FL PMZ (red) and sham-injured astrocytes (black). Open circles show averages and slope of the relationship between pre- and post-TBOA kinetics. Error bars represent SEM.

TC kinetics from cellular filtering artifacts induced by differences in R_m across conditions. To adjust for differences in cell filtering, we performed centroid analysis as described in detail by Diamond (2005) (Fig. 3A, B). The centroid (<t>) is used as a measure of the kinetics of the TC, with larger centroids reflecting slower currents. Briefly, to isolate the glutamate clearance kinetics, we compared TC kinetics ($<t>_{PMZ}$, $<t>_{Sham}$) to the inverse of the rising slope of the TC before and after partially blocking transporters with 10 μM TBOA (Fig. 3B). Inverse TC rising slopes in TBOA were normalized to the slopes before TBOA wash-on, yielding the normalized inverse slope ratio and the resulting relationship between $<t>_{PMZ}$ and $<t>_{Sham}$. The slopes of the relationships pre- and post-10 μM TBOA reflect the isolated glutamate clearance kinetics, with steeper slopes indicating slower clearance. Despite the significantly lower R_m of P7 PMZ astrocytes, the average slopes of P7 PMZ and sham-injured astrocytes were not significantly different ($Slope_{PMZ} = 49.8 \pm 8.02$, $n = 8$; $Slope_{Sham} = 47.03 \pm 15.8$, $n = 6$, $p = 0.47$, Fig. 3C). These data suggest that glutamate clearance by individual astrocytes is unaltered in FL cortex during the latent period. Changes in R_m associated with FL do not mask large differences in glutamate clearance.

3.3. Glutamate transporter expression and distribution are altered by FL

To understand how glutamate uptake systems are altered broadly throughout the cortex by FL, immunofluorescence measurements of glutamate transporters were carried out in the developing (P7) and mature (P28) FL cortex. Brain sections were immunolabeled for GFAP and either GLT-1 or GLAST and wide-field fluorescence images were collected including the microgyrus and PMZ or sham-injured isotopic cortex. 500–800 μm long regions of interest were analyzed laterally through layers IV-VI to quantify GLT-1 and GLAST expression. Measurements of fluorescence intensity were quantified as the average fluorescence through layers IV-VI at a given distance from the start of the region of interest. In FL cortex, regions of interest started at the midline of the microgyrus. In sham-injured cortex, regions started in isotopic cortex. All regions of interest began medially and progressed away from the midline of the cortex. Interestingly, we found that the distribution of both GLT-1 and GLAST is altered by FL during the latent period and in the mature FL cortex (Fig. 4). Additionally, the alterations in the expression of each transporter are spatially and temporally specific. At P7, we found that GLT-1 expression is comparable to sham-injured cortex within the microgyrus, but elevated at the edge of the lesion and in the PMZ ($p < 0.05$ from 260 to 710 μm from the microgyrus midline; Fig. 4A, C, M). GLAST expression, on the other hand, is highest in the center of the microgyrus and decreases outward through the PMZ ($p < 0.05$ from 0 to 510 μm from the microgyrus midline; Fig. 4B, F, N). At P28, both GLT-1 and GLAST are higher in the microgyrus compared to the PMZ. However, in FL compared to sham-injured cortex, GLAST expression is significantly higher throughout the microgyrus and PMZ ($p < 0.05$ from 0 to 760 μm from the microgyrus midline; Fig. 4D, H, Q) while GLT-1 expression is comparable in the microgyrus but lower in the PMZ ($p < 0.05$ from 340 to 900+ μm from the microgyrus midline; Fig. 4C, G, P). Taken together, these data imply that the balance of GLT-1 and GLAST expression is shifted to favor GLT-1 in P7 PMZ and GLAST in the mature PMZ (relative to sham-injured cortex). Importantly, this assessment agrees with recent functional data from our lab demonstrating that TCs in PMZ are more reliant on GLT-1 at P7 and on GLAST at P28 as compared to TCs in sham-injured cortex (Armbruster et al., 2014). Furthermore, when GLT-1 and GLAST expression are compared to GFAP expression in the developing FL cortex (Fig. 4I, J) regions with high GFAP expression have significantly stronger GLAST expression (1.27 ± 0.08 fold change) compared to regions with low GFAP expression (0.96 ± 0.06 fold change, $p < 0.001$). GLT-1 expression, however, is similar across high (1.01 ± 0.08 fold change) and low GFAP regions (1.00 ± 0.07 fold change, $p = 0.3$, Fig. 4O). There is no correlation between GFAP immunoreactivity and either GLT-1 or GLAST in the mature FL cortex (Fig. 4K, L, R), which is likely explained by an overall decrease in GFAP immunoreactivity in FL cortex from P7 to P28.

3.4. Clearance of synaptically-released glutamate by individual astrocytes is unaltered in the mature PMZ

Recent studies of astrocytic glutamate regulation after FL have indicated that, in the mature FL cortex, reduced astrocytic glutamate uptake may contribute acutely to hyperexcitability. Because uncaging-TCs were not altered in the FL cortex, we next examined TCs evoked by synaptic stimulation. We also investigated TCs in the microgyrus, an area which does not generate epileptiform electrical activity (Jacobs et al., 1996). Recording within the microgyrus provides an interesting window into FL hyperexcitability because the microgyrus itself is malformed but not hyperexcitable. Comparing synaptically-released glutamate transients (STCs) between the microgyrus and PMZ could reveal differences in glutamate release and/or clearance mechanisms between the two regions that contribute to PMZ hyperexcitability. To measure STCs, P28 astrocytes in the PMZ, microgyrus, and isotopic sham-injured cortex were patch-clamped and TCs were evoked by electrical stimulation of the white matter below the recording electrode (Fig. 5A). Threshold stimulation intensity was determined on a cell-by-cell basis as the minimum 50 μs current pulse required to evoke a resolvable (5–15 pA) current in astrocytes. STCs were then evoked with 2× threshold stimulation. Recordings were carried out in the presence of Ba^{2+} (100 μM) to eliminate potassium contamination of TCs associated with electrical stimulation. To completely isolate TCs, we applied

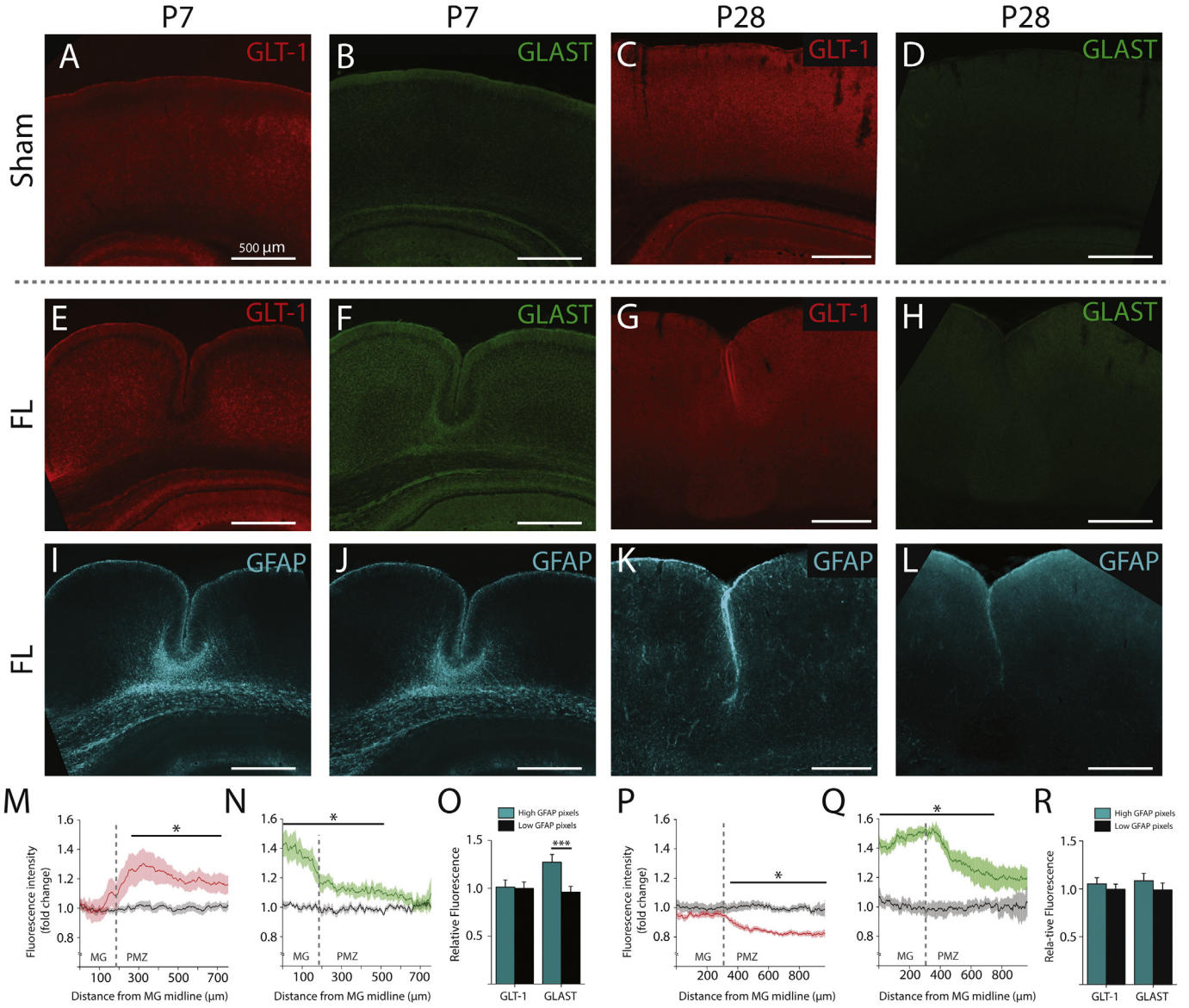

Fig. 4. Glutamate transporter expression and distribution are altered by FL. A–D, Pseudo-colored epifluorescence images of GLT-1 (red) and GLAST (green) immunoreactivity in sham-injured cortex at P7 (left) and P28 (right). E-H, Pseudo-colored epifluorescence images of GLT-1 (red) and GLAST (green) immunoreactivity in FL cortex at P7 (left) and P28 (right) showing the microgyrus and PMZ. I-L, Pseudo-colored epifluorescence images of GFAP co-stain (cyan) in the same FL sections shown in E-H. M, Average fold change in GLT-1 immunoreactivity across the deep layers of the P7 cortex (compared to isotopic sham-injured cortex) at specified distances from the midline of the microgyrus (MG). N, Average fold-change in GLAST immunoreactivity across the deep layers of the P7 cortex (compared to isotopic sham-injured cortex) at specified distances from the midline of the microgyrus (MG). O, Relative GLT-1 and GLAST expression in regions of high GFAP expression (cyan bars) compared to regions with low GFAP expression (black bars) in P7 cortex. High and low GFAP regions were defined by a GFAP expression threshold applied on a pixel-by-pixel basis. P, Average fold-change in GLT-1 immunoreactivity across the deep layers of the P28 cortex (compared to isotopic sham-injured cortex) at specified distances from the midline of MG. Q, Average fold change in GLAST immunoreactivity across the deep layers of the P7 cortex (compared to isotopic sham-injured cortex) at specified distances from the midline of MG. Q, Relative GLT-1 and GLAST expression in regions of high GFAP expression (cyan bars) compared to regions with low GFAP expression (black bars) in P28 cortex. Error bars represent SEM, scale bars are 500 µm, $^{*}p < 0.05$, $^{***}p < 0.001$, two-sample t-test.

TBOA (100 µM) at the end of each experiment and subtracted the TBOA-dependent component of each evoked response. Fig. 5B shows peak-normalized average STCs from astrocytes in PMZ, microgyrus, and sham-injured cortex. STCs from PMZ (n = 7), microgyrus (n = 6), and sham-injured astrocytes (n = 6) showed similar decay kinetics (PMZ: 18.7 ± 2.17 ms, microgyrus: 17.1 ± 1.12 ms, sham: 16.0 ± 1.52 ms), suggesting that glutamate is cleared from the extracellular space at the same rate by astrocytes across regions (Fig. 5B, C). The latency from stimulation to peak current, however, was longer in microgyral astrocytes (14.5 ± 0.86) than in sham-injured astrocytes (10.9 ± 1.19, $p < 0.05$, Fig. 5B inset and 3D). The R_m of sham-injured and microgyral astrocytes is similar (Sham: 2.07 ± 0.37 MΩ, MG: 1.65 ± 0.22 MΩ, $p = 0.36$) suggesting that the increased latency is not influenced by changes in R_m. Taken together these results demonstrate that individual astrocytes clear endogenous glutamate from the microgyrus, the PMZ, and isotopic sham-injured cortex at the same rate, though the initiation of the transporter current after electrical stimulation is delayed in the microgyrus.

3.5. FL alters synaptically-evoked TC amplitude and the stimulation intensity required to evoke a TC

We next examined the amplitude of STCs (at 2× threshold stimulation) in the PMZ, the microgyrus, and sham-injured cortex. Fig. 6A shows the average STCs without peak normalization. Though the kinetics of the STCs were similar in PMZ, microgyral, and sham-injured

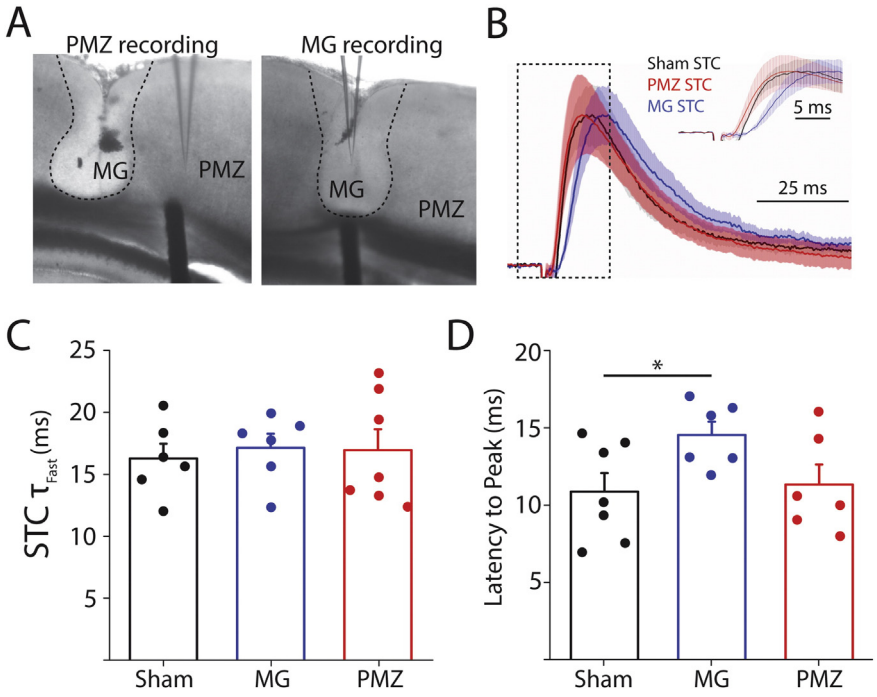

Fig. 5. Synaptically-evoked glutamate transporter current decay kinetics are not affected by FL, but the latency to peak is increased in the microgyrus. A, DIC images of lesions showing placement of stimulator and recording electrodes for PMZ (left) and microgyral (MG) recording (right). Edge of the lesion is denoted by dashed line. B, Peak normalized averages of all PMZ (red), MG (blue), and sham-injured (black) STCs with shaded area showing ± SEM. Inset shows an expansion of the area show in the dashed box. C, Average (bar) and individual (circle) fast decay time constants of STCs evoked in sham-injured, MG, and PMZ astrocytes. D, Average (bar) and individual (circle) latencies to STC peaks in sham-injured, microgyral, and PMZ astrocytes. Error bars represent SEM, *$p < 0.05$, two-sample t-test.

cortex, the amplitudes of STCs were consistently larger in the PMZ (348.7 ± 86.7 pA) compared to sham-injured cortex (98.28 ± 23.3, $p < 0.05$, Fig. 6A, B). The stimulation intensity required to evoke a threshold STC varied widely from 0.01–1 mA in sham-injured cortex (mean = Fig. 6C, D). In the FL cortex, however, the stimulus intensity required to evoke a threshold STC was significantly smaller and varied extremely little in both PMZ (0.02–0.16 mA, 0.09 ± 0.03 mA, $p < 0.05$) and the microgyrus (0.03–0.13 mA, 0.07 ± 0.01 mA, $p < 0.05$; Fig. 6C). Importantly, the amplitudes of the currents evoked at threshold stimulation were similar between PMZ (10.9 ± 0.73 pA), microgyral (12.2 ± 3.15 pA), and sham-injured astrocytes (11.0 ± 1.44 pA; Fig. 6D). The ratio between 2× and 1× threshold stimulation was then calculated (Fig. 6E). This ratio was significantly greater in the PMZ (29.1 ± 5.59) compared to sham-injured cortex (14.5 ± 5.23, $p < 0.001$). The larger ratio and smaller threshold stimulation intensity in the PMZ is likely related to changes in glutamatergic inputs to the area. For example, an increase in the number of subcortical inputs and excitatory synapses in the PMZ is well-documented after FL. Increased glutamatergic inputs may cause greater increases in glutamate release with increasing stimulus intensity in the PMZ, thus contributing to greater scaling of PMZ STCs with stimulus intensity.

3.6. Paired analysis of STCs and FTCs in individual astrocytes shows consistently faster kinetics of FTCs

To examine whether FL induces systematic differences in the handling of synaptically-released versus exogenous glutamate, we recorded paired STCs and FTCs from individual astrocytes (Fig. 7A). Thresholds for electrical stimulation were set as described previously and STCs were evoked with 2× threshold stimulation. Electrical stimulation was alternated with laser photolysis on the astrocyte cell body at a frequency of 0.1 Hz. Recordings were carried out in the presence of Ba^{2+} to isolate TCs. The complete block of both the STC and the FTC in TBOA further confirmed TC specificity. When STCs and FTCs were compared on a cell-by-cell basis, FTCs regularly exhibited faster decay kinetics than STCs (Fig. 7B). The effect was small but consistent across cells and was similar in the PMZ (STC: 18.7 ± 2.17 ms, FTC: 12.9 ± 0.90 ms, $n = 7$, $p < 0.01$), microgyrus (STC: 17.1 ± 1.12 ms, FTC: 13.2 ± 0.68 ms, $n = 7$, $p < 0.05$), and sham-injured cortex (STC: 16.0 ± 1.52 ms, FTC: 12.2 ± 0.69 ms, $n = 7$, $p < 0.01$). The latency-to-peak was also consistently delayed in STCs relative to paired FTCs in the PMZ (STC: 11.3 ± 1.29 ms, FTC: 5.49 ± 0.36 ms, $n = 6$, $p < 0.001$), microgyrus (STC: 14.5 ± 0.86 ms, FTC: 6.00 ± 0.17 ms, $n = 6$, $p < 0.001$), and sham-injured astrocytes (STC: 10.9 ± 1.19 ms, FTC: 5.24 ± 0.40 ms, $n = 7$, $p < 0.01$, Fig. 7C). This is expected because action potential propagation along axons followed by synaptic release and extracellular diffusion imposes a delay between electrical stimulation and glutamate release in STCs, while uncaging releases glutamate directly, with no delay, in the case of FTCs. Additionally, as we observed earlier, the latency-to-peak of STCs was significantly longer in the microgyrus than in sham-injured cortex ($p < 0.05$). However, for paired FTCs there was no significant difference in the latency to peak between microgyral and sham-injured astrocytes ($p = 0.13$). This discrepancy implies that altered glutamatergic inputs to the microgyrus are responsible for the slower latencies in microgyral STCs.

4. Discussion

In this study, we examined in detail the effects of neonatal freeze lesion (FL) on the maturation of glutamate uptake and astrocyte R_m in the cortex. We report that functional glutamate uptake, as measured by transporter current (TC) decay time, is normal in both neonatal and mature astrocytes from the PMZ of freeze lesioned rats. This refutes the idea that individual astrocytes have a uniformly

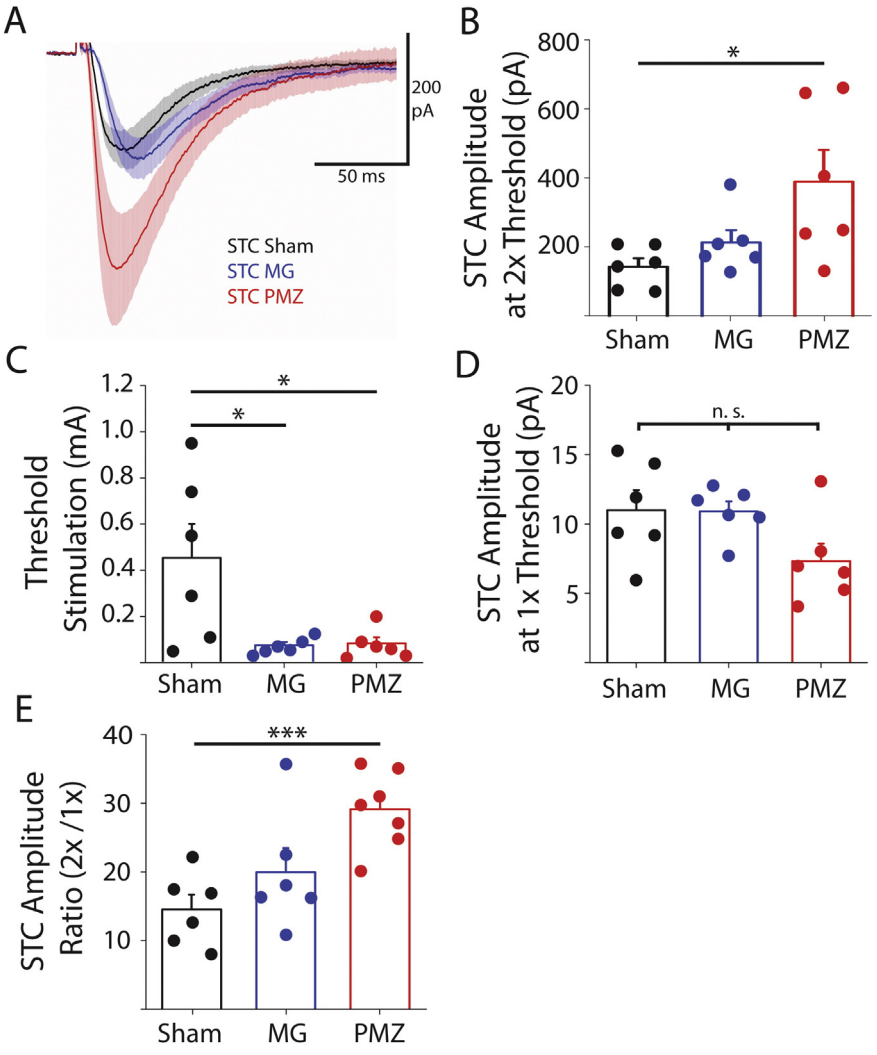

Fig. 6. Synaptically-evoked glutamate transporter current amplitudes are greater in paramicrogyral zone though threshold stimulation intensity is lower. A, Average STCs from PMZ (red), microgyral (MG, blue), and sham-injured (black) astrocytes. Shaded area shows SE. B, Averages (bars) and individual amplitudes of STCs with stimulation intensity at 2× threshold. C, Averages (bars) and individual threshold stimulation intensities. D, Averages (bars) and individual amplitudes of STCs with stimulation intensity at 1× threshold. E, Averages (bars) and individual ratios of STC amplitudes at 2× threshold relative to 1× threshold. Error bars represent SEM, *$p < 0.05$, **$p < 0.01$, ***$p < 0.001$, two-sample t-test.

impaired ability to transport glutamate. In light of other recent works, it suggests a potential heterogeneity in glial function following neonatal brain insult.

Glutamate transporter immunoreactivity varies regionally within the malformed cortex, based on both age and location. This suggests that even though functional glutamate uptake is generally unchanged, transport may rely on different EAATs in FL cortex. Our previous work is consistent with this finding (Armbruster et al., 2014) and suggests an underlying disruption in astrocyte maturation following FL. Indeed, the development of astrocyte R_m is also altered by FL. Astrocytes in the neonatal brain normally have relatively high R_m compared to adult astrocytes. Following FL, however, we found that neonatal astrocytes have a lower R_m, consistent with a more mature phenotype. Finally, our data are consistent with other studies implicating increased glutamatergic input as a potential mechanism of hyperexcitability in FL cortex (Jacobs et al., 1999b; Jacobs and Prince, 2005). Together, our findings suggest that changes in excitation may be a component of FL network pathology, independent of decreased glutamate transport by individual astrocytes.

4.1. Glutamate uptake through FL development and in mature FL cortex

A number of studies suggest that disruptions in glutamatergic signaling occur in human DCMs and in animal models. Changes in the projections of excitatory inputs, increases in excitatory synaptic signaling, and changes in astrocyte number and function have all been reported (Armbruster et al., 2014; Dulla et al., 2012; Jacobs et al., 1999b; Jacobs and Prince, 2005). Evidence from the FL model suggests that glutamate uptake may be altered in the PMZ (S. L. Campbell and Hablitz, 2008; Dulla et al., 2012) and more recent studies indicate that individual astrocytes are less capable of transporting glutamate in adult FL cortex (Campbell et al., 2014). Importantly, questions remain about whether these changes are specific to a subset of astrocytes and whether changes in individual astrocytes correspond to changes in the handling of extracellular glutamate during FL development. Using UV-uncaging of glutamate, we observed astrocyte TCs with normal kinetics and amplitudes in the FL cortex. This approach gives information regarding the amount of functional glutamate transport and changes in the extracellular space within the astrocyte domain. It does not, however, provide information

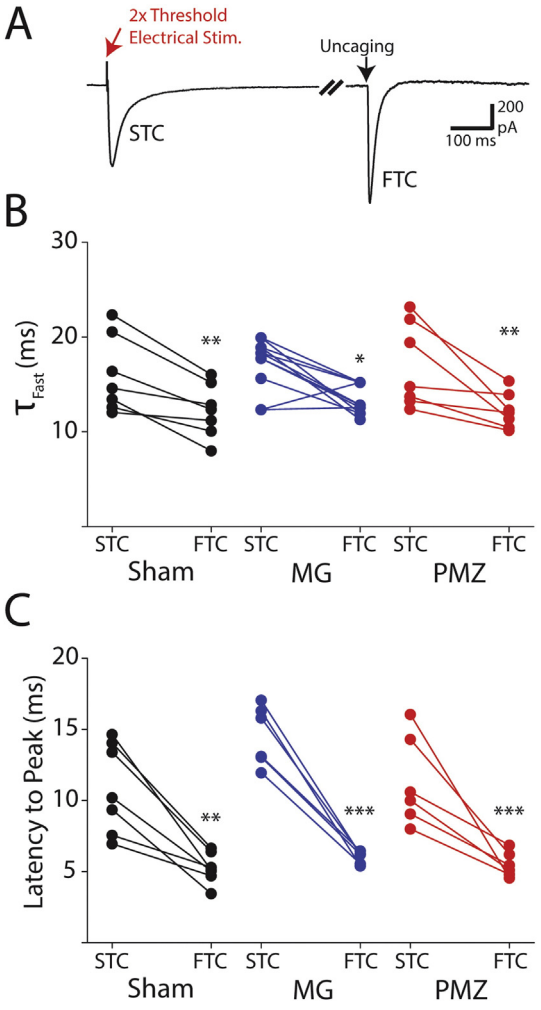

Fig. 7. Paired analysis of STCs and FTCs in individual astrocytes shows consistently faster kinetics of FTCs and confirms lack of lesion dependent change in glutamate uptake kinetics. A, Representative trace from a single P28 PMZ astrocyte showing paired electrically-evoked STCs and uncaging-evoked FTCs. Break = 7.5 s. B, Paired fast time constants of STC and FTC decays from individual sham-injured (black), microgyral (MG, blue) PMZ astrocytes (red). C, Paired peak latencies of STCs and FTCs from individual sham-injured (black), microgyral (blue), and PMZ astrocytes (red). Error bars represent SEM, $^{**}p < 0.01$, $^{***}p < 0.001$, paired t test.

about glutamate handling in the native synaptic environment, nor does it account for developmental or injury-induced changes in glutamate release, which likely contribute to hyperexcitability.

To account for FL effects on glutamate release and handling within the synaptic environment, we examined the astrocytic uptake of synaptically-released glutamate. Again, we found similar TC kinetics in the FL and sham-injured cortex. Using synaptic stimulation, however, we observed TCs that were significantly larger in the PMZ compared to sham-injured cortex. Increased synaptically-evoked TC amplitude and unchanged uncaging-evoked TC amplitude together suggest that there are changes in endogenous glutamate release rather than astrocyte glutamate uptake. In line with this hypothesis, the threshold to evoke a synaptic TC was significantly lower in the FL cortex, indicating that neuronal glutamatergic inputs are increased in number or that ascending axons are more easily activated (Brill and Huguenard, 2010; Dulla et al., 2012; Jacobs et al., 1999c). The delayed onset of synaptically-evoked TCs in the microgyrus also supports a model of FL pathology which includes large-scale reorganization of afferent excitatory fibers (Jacobs et al., 1999b; Jacobs et al., 1999c). However, it is also possible that changes in astrocyte morphology in relation to synapses or changes in the subcellular distribution of transporters may contribute to the delay. Taken together, our studies show that there is a large population of astrocytes that are robustly capable of removing extracellular glutamate in the PMZ. It remains to be determined, however, whether decreased astrocytic density or altered EAAT reliance in the PMZ affects glutamate handling. Earlier imaging studies do support a decreased ability to take up glutamate in deep cortical layers within the PMZ (Dulla et al., 2012), but the current study indicates that decreased glutamate clearance is not due to individual astrocytes losing the ability to transport glutamate.

4.2. Glutamate transporter expression and distribution

Studies of glutamate transport in human malformed cortex have been limited to biochemical and histopathological techniques. They have shown that overall expression of GLT-1 is decreased in dysplastic cortex and that the distribution of transporters appears more diffuse (Ulu et al., 2010). Previous electrophysiological studies in the FL model have investigated whether transport may rely on different EAATs, but direct immunolabeling of GLT-1 has only recently been qualitatively examined (Campbell et al., 2014). Immunolabeling of GLAST remains unreported in FL. Thus, to understand how glutamate uptake systems are altered broadly by injury, we measured the immunoreactivity of glutamate transporters in the developing and mature FL cortex. We found that expression of GLT-1 and GLAST are significantly altered during the latent period and in mature FL cortex relative to sham-injured cortex. Furthermore, the distribution of GLT-1 and GLAST varies greatly across the malformation and changes substantially over the course of FL development. For example, at P7 GLT-1 expression is elevated in the PMZ with the peak expression near the PMZ/MZ border. This is in contrast to the expression pattern of GLAST in P7 FL cortex which is highest at the center of the microgyrus and decreases outward through the PMZ. These changes suggest an increase in the ratio of GLT-1 to GLAST in the PMZ and are supported by our recent study showing an increased reliance of glutamate transport on GLT-1 in P7 PMZ astrocytes (Armbruster et al., 2014).

In the mature FL cortex, we have found that GLT-1 expression is decreased sharply starting at the border of the PMZ. Within the microgyrus, GLT-1 expression is normal while GLAST expression is strongly elevated. Moving outward through the PMZ, GLAST expression decreases relative to the microgyrus but remains elevated relative to sham-injured cortex. The increased expression of GLAST potentially counteracts decreases in GLT-1 expression in the mature PMZ. Importantly, an increase in the expression of GLAST relative to GLT-1 is in agreement with a recent study demonstrating that TCs in the mature FL cortex are less dependent on GLT-1 (Armbruster et al., 2014). In the mature PMZ, the parallel increase in GLAST and decrease in GLT-1 suggests that changes in transporter expression are not entirely compensatory in response to increased excitability (which would increase expression of both transporters), nor are they the result of astrocyte hypertrophy or a decrease in astrocyte number (which would also likely affect the immunoreactivity of both transporters in a similar way).

It should be noted that a recent study using the FL model found GLT-1 protein and mRNA expression to be unchanged in the mature PMZ (Campbell et al., 2014). However, Western blots and mRNA analyses, which are necessarily regional averages, may not register spatially specific differences in glutamate transporters. Measuring immunoreactivity provides much greater spatial resolution, which is critical for examining protein expression across the heterogeneous microgyrus and PMZ. However, the intensity of immunofluorescence is subject to external factors besides protein expression, including tissue water content and staining conditions. Those caveats must be considered in interpreting our immunostaining results. Ultimately, the current findings may be confirmed with mass-spectrometry proteomics, single cell transcript

analysis, or microdissection and immunoblotting, though these experiments are outside the scope of the current study.

4.3. Astrocyte membrane resistance

Astrocytes are characterized by their hyperpolarized resting membrane potential, low R_m, and passive membrane properties created by high expression of potassium channels. Immature astrocytes, however, have a high R_m due to their decreased expression of potassium channels. Here we have found that the R_m of astrocytes identified by SR-101 labeling is altered during FL development, but is ultimately unchanged in the mature FL cortex. Specifically, during the latent period, astrocyte R_m is lower in the PMZ than in isotopic sham-injured cortex. In both regions, astrocyte R_m decreases significantly over the course of development. In the mature PMZ and sham-injured cortices, R_m is similarly low. This early maturation of R_m may indicate that astrocytes are better able to buffer potassium at an earlier developmental time point following injury. These findings stand in contrast to the recent study in which >80% of astrocytes in the mature PMZ exhibited the immature characteristics, high R_m and voltage-dependent currents (Campbell et al., 2014).

4.4. Heterogeneity of astrocytes in FL

Injuries during development and in the mature cortex induce both astrocyte reactivity and proliferation. First, heterogeneity across cells based on reactivity is known to exist. In the FL model, astrocyte reactivity is highest immediately after the time of injury, but remains elevated into adulthood (Shimizu-Okabe et al., 2007). While many astrocytes express GFAP in the FL cortex, other cells which express astrocyte markers (ALDH1L1) do not (Dulla et al., 2012). This variability in reactivity state may indicate significant functional heterogeneity. Next, throughout FL development, proliferation occurs in a subset of astrocytes (as measured by BrdU labeling), generating astrocytes which have different electrophysiological properties based on maturation state (Bordey et al., 2001). This suggests a second axis of heterogeneity in the FL cortex based on the relative maturity of any given astrocyte. More recently generated astrocytes likely have a more immature phenotype and can be found within a mixed population of more mature astrocytes. Lastly, heterogeneity in astrocyte distribution has been seen in the FL cortex; deep cortical layers of the PMZ have a significantly decreased density of astrocytes (Armbruster et al., 2014; Dulla et al., 2012), perhaps due to injury occurring during normal developmental proliferation of cortical astrocytes. Overall, the functional and morphological heterogeneity of astrocytes has been well documented after injury, and in the FL model in particular.

4.5. Complications in the functional characterization of glutamate uptake in the FL model

We have observed intact astrocytic glutamate uptake throughout PMZ development and in the mature microgyrus and PMZ. Additionally, during PMZ development (at P7) astrocyte R_m is low, which is a characteristic membrane property of more mature astrocytes. Furthermore, we demonstrate that the relative expression of glutamate transporters is altered during FL development to favor GLT-1 in the P7 PMZ and GLAST in P28 PMZ. These findings are consistent with previous studies from our group and with other studies of SR-101-identified astrocyte properties in the epileptic brain showing robust glutamate transport (Takahashi et al., 2010). Studies which do not utilize SR-101 labeling, or other cell-labeling strategies to identify astrocytes, however, have concluded that individual astrocytes in the FL cortex have immature properties (increased Rm, non-passive membrane properties, decreased capacitance, decreased potassium buffering, decreased gap junction coupling) and little to no glutamate uptake capacity (Bordey et al., 2001; Campbell et al., 2014). We suspect that these studies arrive at different conclusions because they use different strategies to identify astrocytes. Identifying astrocytes is complex, especially in the neonatal and injured brain, when astrocyte heterogeneity is increased. After FL only a subset of astrocytes becomes proliferative. These astrocytes likely have different electrophysiological properties and glutamate transport capacities. Importantly, SR-101 may selectively load astrocytes depending on their proliferation or reactivity state. It is possible that confusion regarding the role of astrocytes in PMZ development and hyperexcitability stems from different studies selectively assaying different populations of cells. The possibility of an astrocyte selection bias between our study and others raises questions of how astrocytes are identified, particularly after injury. Thus, carefully defining astrocyte subtypes and identifying reliable selection criteria are critical aspects of studies examining individual astrocytes after injury. Furthermore, changes in R_m complicate the interpretation of TC data. R_m is decreased in P7 FL astrocytes (Fig. 2), but TC kinetics remains constant (Fig. 1). This suggests a possible increase in glutamate transporter surface expression. On the other hand, centroid analysis of TC kinetics, aimed at removing filtering artifacts created by changes in R_m, did not reveal differences in glutamate uptake by FL astrocytes (Fig. 3). Clearly, more investigation, including direct biochemical measurements of surface GLT1 and GLAST would be helpful. Lastly, it is important to note that single-cell analysis of glutamate uptake may not directly correlate to population level control of extracellular glutamate, as other factors such as astrocyte density, morphology, and extracellular tortuosity all contribute to glutamate dynamics.

5. Conclusions

In summary, this study shows that although neonatal injury in the FL model alters astrocyte development of R_m and EAAT expression, there is, nevertheless, robust glutamate uptake by individual astrocytes throughout FL development. The spatial differences in EAAT expression that we observed in FL cortex suggest that (1) during FL development, astrocytic glutamate uptake relies more on GLT-1 in the PMZ than in sham-injured cortex and (2) in the mature PMZ, astrocytes rely more on GLAST than in sham-injured cortex. Importantly, this assessment is supported by recent electrophysiological evidence demonstrating that the relative contribution of GLT-1 and GLAST to transporter currents is altered by FL (Armbruster et al., 2014). Based on data from animal models and from human DCMs, we support a model in which neonatal insult results in enhanced excitatory input, as well as changes in astrocyte density, distribution, proliferation, morphology, and the relative contribution of EAAT subtypes. While these changes may, in fact, lead to dysregulation of bulk glutamate or ambient glutamate levels, our findings indicate that a uniform loss of astrocytic glutamate uptake by individual cells is not responsible for hyperexcitability in FL cortex.

Acknowledgments

This work was supported by the Epilepsy Foundation (CD), National Institute of Neurological Disease and Stroke R01-NS076885 (CD), Synapse Neurobiology Training Grant (EH, NINDS T32-NS061764, M. Jacob, P.I.), Tufts Center for Neuroscience Research (P30 NS047243), and The Norwegian Research Council (240844, NCD). The authors would like to thank Dr. Moritz Armbruster for helpful discussions, Danielle Croker for technical help, and Jenny Koenig for help with the manuscript.

References

Andresen, L., Hampton, D., Taylor-Weiner, A., Morel, L., Yang, Y., Maguire, J., Dulla, C.G., 2014. Gabapentin attenuates hyperexcitability in the freeze-lesion model of developmental cortical malformation. Neurobiol. Dis. 71, 305–316.

Armbruster, M., Hampton, D., Yang, Y., Dulla, C.G., 2014. Laser-scanning astrocyte mapping reveals increased glutamate-responsive domain size and disrupted maturation of glutamate uptake following neonatal cortical freeze-lesion. Front. Cell. Neurosci. 8.

Aronica, E., Becker, A.J., Spreafico, R., 2012. Malformations of cortical development. Brain Pathol. 22 (3), 380–401.
Barkovich, A., Kuzniecky, R., Jackson, G., Guerrini, R., Dobyns, W., 2005. A developmental and genetic classification for malformations of cortical development. Neurology 65 (12), 1873–1887.
Bordey, A., Lyons, S.A., Hablitz, J.J., Sontheimer, H., 2001. Electrophysiological characteristics of reactive astrocytes in experimental cortical dysplasia. J. Neurophysiol. 4 retrieved from http://www.ncbi.nlm.nih.gov/pubmed/11287494.
Brill, J., Huguenard, J.R., 2010. Enhanced infragranular and supragranular synaptic input onto layer 5 pyramidal neurons in a rat model of cortical dysplasia. Cereb. Cortex 12 retrieved from http://www.ncbi.nlm.nih.gov/pubmed/20338974.
Campbell, S., Hablitz, J.J., Olsen, M.L., 2014. Functional changes in glutamate transporters and astrocyte biophysical properties in a rodent model of focal cortical dysplasia. Front. Cell. Neurosci. 8.
Campbell, S.L., Hablitz, J.J., 2008. Decreased glutamate transport enhances excitability in a rat model of cortical dysplasia. Neurobiol. Dis. 2 retrieved from http://www.ncbi.nlm.nih.gov/pubmed/18674619.
Cavus, I., Kasoff, W.S., Cassaday, M.P., Jacob, R., Gueorguieva, R., Sherwin, R.S., ... Abi-Saab, W.M., 2005. Extracellular metabolites in the cortex and hippocampus of epileptic patients. Ann. Neurol. 57 (2), 226–235.
Danbolt, N.C., 2001. Glutamate uptake. Prog. Neurobiol. 1 retrieved from http://www.ncbi.nlm.nih.gov/pubmed/11369436.
Diamond, J.S., 2005. Deriving the glutamate clearance time course from transporter currents in CA1 hippocampal astrocytes: transmitter uptake gets faster during development. J. Neurosci. 11 retrieved from http://www.ncbi.nlm.nih.gov/pubmed/15772350.
Diamond, J.S., Bergles, D.E., Jahr, C.E., 1998. Glutamate release monitored with astrocyte transporter currents during LTP. Neuron 2 retrieved from http://www.ncbi.nlm.nih.gov/pubmed/9728923.
Dulla, C.G., Tani, H., Brill, J., Reimer, R.J., Huguenard, J.R., 2012. Glutamate biosensor imaging reveals dysregulation of glutamatergic pathways in a model of developmental cortical malformation. Neurobiol. Dis. http://www.ncbi.nlm.nih.gov/pubmed/22982711.
Dvorák, K., Feit, J., 1977. Migration of neuroblasts through partial necrosis of the cerebral cortex in newborn rats-contribution to the problems of morphological development and developmental period of cerebral microgyria. Histological and autoradiographical study. Acta Neuropathol. 3 retrieved from http://www.ncbi.nlm.nih.gov/pubmed/899721.
Fonnum, F., 1984. Glutamate: a neurotransmitter in mammalian brain. J. Neurochem. 42 (1), 1–11.
Guerrini, R., Dobyns, W.B., 2014. Malformations of cortical development: clinical features and genetic causes. The Lancet Neurology 13 (7), 710–726.
Hablitz, J.J., DeFazio, T., 1998. Excitability changes in freeze-induced neocortical microgyria. Epilepsy Res. 1-2 retrieved from http://www.ncbi.nlm.nih.gov/pubmed/9761310.
Halassa, M.M., Fellin, T., Takano, H., Dong, J.-H., Haydon, P.G., 2007. Synaptic islands defined by the territory of a single astrocyte. J. Neurosci. 27 (24), 6473–6477.
Hanson, E., Armbruster, M., Cantu, D., Andresen, L., Taylor, A., Danbolt, N.C., Dulla, C.G., 2015. Astrocytic glutamate uptake is slow and does not limit neuronal NMDA receptor activation in the neonatal neocortex. Glia.
Holmseth, S., Dehnes, Y., Huang, Y.H., Follin-Arbelet, V.V., Grutle, N.J., Mylonakou, M.N., ... Bergles, D.E., 2012a. The density of EAAC1 (EAAT3) glutamate transporters expressed by neurons in the mammalian CNS. J. Neurosci. 32 (17), 6000–6013.
Holmseth, S., Scott, H., Real, K., Lehre, K., Leergaard, T., Bjaalie, J., Danbolt, N., 2009. The concentrations and distributions of three C-terminal variants of the GLT1 (EAAT2; slc1a2) glutamate transporter protein in rat brain tissue suggest differential regulation. Neuroscience 162 (4), 1055–1071.
Holmseth, S., Zhou, Y., Follin-Arbelet, V.V., Lehre, K.P., Bergles, D.E., Danbolt, N.C., 2012b. Specificity controls for immunocytochemistry the antigen preadsorption test can lead to inaccurate assessment of antibody specificity. J. Histochem. Cytochem. 60 (3), 174–187.
Jacobs, K.M., Gutnick, M.J., Prince, D.A., 1996. Hyperexcitability in a model of cortical maldevelopment. Cereb. Cortex 3 retrieved from http://www.ncbi.nlm.nih.gov/pubmed/8670677.
Jacobs, K.M., Hwang, B.J., Prince, D.A., 1999a. Focal epileptogenesis in a rat model of polymicrogyria. J. Neurophysiol. 1 retrieved from http://www.ncbi.nlm.nih.gov/pubmed/9914277.
Jacobs, K.M., Kharazia, V.N., Prince, D.A., 1999b. Mechanisms underlying epileptogenesis in cortical malformations. Epilepsy Res. 2-3 retrieved from http://www.ncbi.nlm.nih.gov/pubmed/10515164.
Jacobs, K.M., Mogensen, M., Warren, E., Prince, D.A., 1999c. Experimental microgyri disrupt the barrel field pattern in rat somatosensory cortex. Cereb. Cortex 7 retrieved from http://www.ncbi.nlm.nih.gov/pubmed/10554996.
Jacobs, K.M., Prince, D.A., 2005. Excitatory and inhibitory postsynaptic currents in a rat model of epileptogenic microgyria. J. Neurophysiol. 2 retrieved from http://www.ncbi.nlm.nih.gov/pubmed/15385597.
Kakita, A., Kameyama, S., Hayashi, S., Masuda, H., Takahashi, H., 2004. Pathologic features of dysplasia and accompanying alterations observed in surgical specimens from patients with intractable epilepsy. J. Child Neurol. 19 (3), 341–350.
Kamada, T., Sun, W., Takase, K.-I., Shigeto, H., Suzuki, S.O., Ohyagi, Y., Kira, J.-I., 2013. Spontaneous seizures in a rat model of multiple prenatal freeze lesioning. Epilepsy Res. 105 (3), 280–291.
Marin-Valencia, I., Guerrini, R., Gleeson, J.G., 2014. Pathogenetic mechanisms of focal cortical dysplasia. Epilepsia 55 (7), 970–978.
Morel, L., Higashimori, H., Tolman, M., Yang, Y., 2014. VGluT1+ neuronal glutamatergic signaling regulates postnatal developmental maturation of cortical protoplasmic astroglia. J. Neurosci. 34 (33), 10950–10962.
Nimmerjahn, A., Kirchhoff, F., Kerr, J.N., Helmchen, F., 2004. Sulforhodamine 101 as a specific marker of astroglia in the neocortex in vivo. Nat. Methods 1 (1), 31–37.
Oliet, S.H., Piet, R., Poulain, D.A., 2001. Control of glutamate clearance and synaptic efficacy by glial coverage of neurons. Science 292 (5518), 923–926.
Palmini, A., Gambardella, A., Andermann, F., Dubeau, F., da Costa, J.C., Olivier, A., ... Andermann, E., 1995. Intrinsic epileptogenicity of human dysplastic cortex as suggested by corticography and surgical results. Ann. Neurol. 37 (4), 476–487.
Petr, G.T., Sun, Y., Frederick, N.M., Zhou, Y., Dhamne, S.C., Hameed, M.Q., ... Armsen, W., 2015. Conditional deletion of the glutamate transporter GLT-1 reveals that astrocytic GLT-1 protects against fatal epilepsy while neuronal GLT-1 contributes significantly to glutamate uptake into synaptosomes. J. Neurosci. 35 (13), 5187–5201.
Petroff, O.A., Errante, L.D., Rothman, D.L., Kim, J.H., Spencer, D.D., 2002. Glutamate–glutamine cycling in the epileptic human hippocampus. Epilepsia 43 (7), 703–710.
Raymond, A., Fish, D., Sisodiya, S., Alsanjari, N., Stevens, J., Shorvon, S., 1995. Abnormalities of gyration, heterotopias, tuberous sclerosis, focal cortical dysplasia, microdysgenesis, dysembryoplastic neuroepithelial tumour and dysgenesis of the archicortex in epilepsy. Brain 118 (3), 629–660.
Shimizu-Okabe, C., Okabe, A., Kilb, W., Sato, K., Luhmann, H.J., Fukuda, A., 2007. Changes in the expression of cation-Cl^- cotransporters, NKCC1 and KCC2, during cortical malformation induced by neonatal freeze-lesion. Neurosci. Res. 59 (3), 288–295.
Sisodiya, S., 2000. Surgery for malformations of cortical development causing epilepsy. Brain 123 (6), 1075–1091.
Sofroniew, M.V., 2009. Molecular dissection of reactive astrogliosis and glial scar formation. Trends Neurosci. 32 (12), 638–647.
Takahashi, D., Vargas, J., Wilcox, K., 2010. Increased coupling and altered glutamate transport currents in astrocytes following kainic-acid-induced status epilepticus. Neurobiol. Dis. 40 (3), 573–585.
Tassi, L., Colombo, N., Garbelli, R., Francione, S., Russo, G.L., Mai, R., ... Galli, C., 2002. Focal cortical dysplasia: neuropathological subtypes, EEG, neuroimaging and surgical outcome. Brain 125 (8), 1719–1732.
Ullensvang, K., Lehre, K., Storm-Mathisen, J., Danbolt, N., 1997. Differential developmental expression of the two rat brain glutamate transporter proteins GLAST and GLT. Eur. J. Neurol. 9 (8), 1646–1655.
Ulu, M.O., Tanriverdi, T., Oz, B., Biceroglu, H., Isler, C., Eraslan, B.S., ... Uzan, M., 2010. The expression of astroglial glutamate transporters in patients with focal cortical dysplasia: an immunohistochemical study. Acta Neurochir. 152 (5), 845–853.